



## **Parametric study on the local buckling of high strength steel stub columns under axial compression**

Dileep B. Chandrashekhar<sup>1</sup>, Rachel A. Chicchi<sup>2</sup>

### **Abstract**

High strength structural steel (HS3), which in this context is being defined as steel with a yield strength greater than 100 ksi (690 MPa), has gained popularity worldwide in the building industry due to its superior strength to weight ratio, and satisfactory ductility and toughness. However, the use of HS3 steel for design as a structural member in the US has been limited in part because of the limitations and a lack of guidance within the AISC *Specification*. This study aims to evaluate the local buckling behavior of HS3 stub columns of grades 100 ksi (690 MPa) and 140 ksi (960 MPa) subjected to axial compression. Finite element models were developed and validated in ABAQUS from existing experimental data to capture the local buckling behavior of HS3 wide flange stub columns. A parametric study was conducted to investigate the effect of section slenderness on the local buckling behavior of the column. Three initial column sizes were used, and the web slenderness and the flange slenderness were then varied. The ultimate load capacity of these columns was investigated, and numerical results were then compared with the current local buckling design method in AISC 360 (2016) *Specification* for conventional steel.

### **1. Introduction**

High strength structural steel (HS3) exhibits significantly higher yield strength when compared with conventional mild steel (CMS) – such as ASTM A36 and ASTM A992. It also possesses enough ductility for conventional plastic design and exhibits sufficient toughness and weldability to be used as a structural member (Ban and Shi, 2018). There are many grades of HS3 steel available in the market that are used for construction purposes. The steel properties, national standards, and national codes are periodically updated to include the most optimal properties and the latest advances in research for HS3 steel. China and Europe have developed national standards for the HS3 steel available in their market (65-140ksi). HS3 steel is classified differently in different parts of the world with respect to their national standards. However, it can be classified at large as steel with a yield strength ( $F_y$ ) greater than 65 ksi (450 MPa). In this study, two grades of HS3 steel – 100 ksi (690 MPa) and 140 ksi (960 MPa) – are used to study the local buckling

---

<sup>1</sup> Graduate Research Assistant, University of Cincinnati, <chandrd@mail.uc.edu>

<sup>2</sup> Assistant Professor, University of Cincinnati, <chicchrl@ucmail.uc.edu>

strengths of HS3 stub columns and to study the applicability of the AISC 360 (2016) gravity column design method to design HS3 stub columns.

### 1.1 Motivation

Unlike CMS, HS3 steel has no defined yield plateau. Fig. 1 shows the comparison of the engineering stress-strain relation between HS3 and CMS steel. HS3 steel has a higher yield to tensile strength ratio including higher resistance to loading without increasing the amount of steel. (Shi, Hu, and Shi, 2014). HS3 steel exhibits lower ratios of residual compressive stresses to yield strength of the steel. Because of these differences and others, it is unreasonable to simply apply conventional design methods to HS3 structures without analysis and/or testing. There is a strong need to study the applicability of current design methods for the design of HS3 steel members.

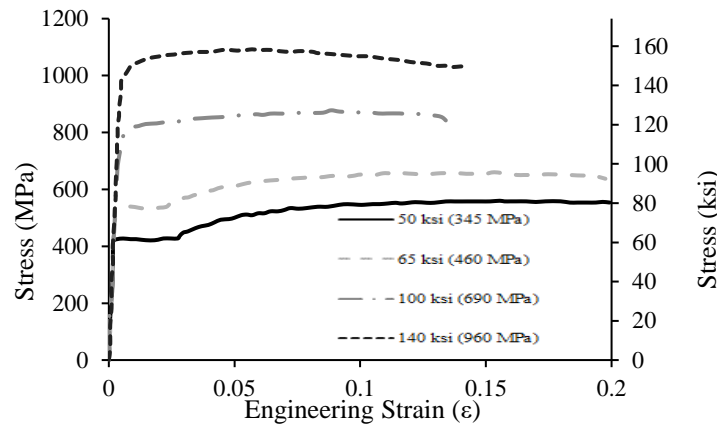


Figure 1: Stress-strain curves of HS3 and CMS - (Ban and Shi, 2018)

A study was previously conducted by Akhtar and Chicchi (2021) to examine the behavior of HS3 wide flange columns under flexural buckling. This work will build upon that previous study to explore local buckling effects in HS3 stub columns through data obtained from numerical simulations and experimental studies. It also studies the applicability of the AISC 360 (2016) local buckling design equations for the HS3 column. Axially-loaded wide flange built-up gravity stub columns with yield strengths of 100 and 140 ksi were studied to obtain their local buckling strengths. Stub columns were selected to be studied because of the ease in capturing the local buckling effects in the HS3 steel.

### 1.2 Previous Studies

Usami and Fukumoto (1982; 1984) studied HS3 stub columns fabricated from 65 ksi (460 MPa) to 100 ksi (690 MPa) grades and performed axial compression tests on built-up box-section stub columns with relatively large width-to-thickness ratios. All the specimens tested were subjected to either concentric or eccentric axial loading through the axial compression test. A formula was proposed for estimating the ultimate stress after local buckling. This formula approach provided satisfactory predictions for columns with large width-to-thickness ratios but was not consistent for columns with small width-to-thickness ratios. In columns with large width-to-thickness ratios and small section slenderness, the mode of failure was usually due to the crippling of flanges and webs at a particular location due to the high axial load. Sometimes, this mode of failure occurred at two or more points, usually at the center and one-fourth location of the length of the column.

Shi et al. (2014) performed experimental research and validated the FE model established by the ANSYS software on the local buckling behavior of both built-up box-section and wide flange section columns made of 67 ksi HS3 steel. The experimental results showed that the local buckling stress, the ultimate stress, and the stress ratio (the ratio of local buckling stress to ultimate stress) decreased with the increase in the width-to-thickness ratio of the plates. This indicated that the local buckling mode had occurred even before the steel had yielded and contributed to determining the ultimate strength of the column. The post-buckling strength of the column increased with the increase in the width-to-thickness ratio. On comparing the results of the experiment and the FE model with that of the estimates from different codes, it was found that the strength of box specimens was overpredicted. In contrast, flanges of the wide flange section column were overly conservative for the case of a relatively high width-to-thickness ratio. The results showed that AISC 360 (2010) and Eurocode 3 (2007) predicted a more accurate ultimate load than the GB50017 (2003) - Chinese code.

Shi et al. (2015) studied the local buckling behavior of 140 ksi (960 MPa) HS3 stub columns by performing experimental axial compression tests with both wide flange section and box-section columns. They then validated their experimental model with a FE analysis in ANSYS. It was found that the design methods in AISC 360 (2010) and Eurocode 3 (2007) overpredicted the strength when the width-to-thickness ratio was comparatively smaller. But with the increase of the width-to-thickness ratio, both design standards were found to be overly conservative. Shi et al. (2016) also established a FE model and found that the design methods in AISC 360 (2010), Eurocode 3 (2007), and GB50017 (2003) were inconsistent with the existing experimental results. Thus, they proposed new design formulas for predicting the post-buckling ultimate stress and the local buckling stress of the column. Fig. 2 shows the flanges of the test column buckling, which was the failure mode observed during testing.

Cao et al. (2020) studied the local buckling behavior of 120 ksi (800 MPa) HS3 stub columns subjected to axial compression. The experimental results showed that the design methods in GB50017 (2017), Eurocode 3 (2007), and AISC 360 (2016) slightly overestimated the ultimate load-bearing capacity of the built-up I- section columns. Cao et al. (2021) performed stub column tests and validated the FE model on three different kinds of HS3 columns of grade 120 ksi. Ninety-four different FE models were modeled to estimate the ultimate load-carrying capacity of the specimen. It was found that the current specifications – (Eurocode 3 (2007) and AISC 360 (2016)) slightly underestimated the ultimate load of the 120 ksi HS3 built-up wide flange section members.



Figure 2: Local buckling mode observed in stub column. (Shi et al., 2015)

## 2. Numerical Modeling

ABAQUS (Dassault Systemes, 2018), a finite element analysis software, was used to simulate the local buckling behavior of HS3 stub columns. The experimental results of Shi et al. (2015) for the 140 ksi stub column, Cao et al. (2020) for the 120 ksi stub column, and Sun et al. (2019) for the 100 ksi stub column were used to benchmark the numerical model. A total of four stub columns were modeled in ABAQUS, which are identified as I1 through I4. Each stub column was partitioned to enable proper residual stress distribution along the cross-section of the built-up wide flange section. The column was modeled using solid elements with dimensional properties consistent with the experimental specimens, as shown in Table 1 and Fig. 3. Welds in the wide flange section were modeled as a part of the wide flange section with the same properties as that of the wide flange section. This was done for ease of modeling and because the welds did not fail during the experimental testing. The specimen cross-sections and results will be presented in metric units because these were the units used in the experiments.

Table 1: Dimensions of the developed FE model

Specimen ID	$F_y$ (ksi)	$L^1$ (mm)	B (mm)	H (mm)	b (mm)	$h_o$ (mm)	$t_r$ (mm)	$t_w$ (mm)	$t_e$ (mm)
I1	140 (960 MPa)	400.3	210.0	212.3	98.1	184.4	13.93	13.88	6
I2	140 (960 MPa)	500.2	267.0	266.0	126.5	238.1	13.96	13.96	6
I3	120 (800 MPa)	549.0	309.3	244.0	150.99	114.65	7.35	7.31	6
I4	100 (690 MPa)	417.5	99.35	199.37	47.19	189.41	4.98	4.98	6

1.  $L$ - is the length of the stub column; 1 inch =25.4 mm

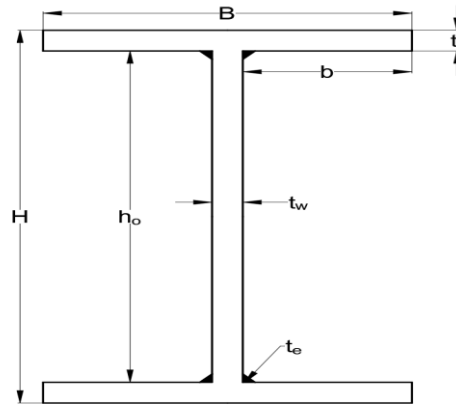


Figure 3: Typical dimensional notations for the cross-sections modeled

The material for the stub column in ABAQUS was modeled as an isotropic material with both elastic and plastic properties. A multilinear kinematic material model was employed for material modeling based on the benchmarked studies. The wide flange stub column in the benchmarked studies was simply supported with pinned-pinned end condition at one end and pinned-roller end condition at the other. The FE model was constrained as pinned on each face to a single point at the centroid of the cross-section with coupling kinematic constraint. The FE model was meshed with a C3D8R (8 node linear brick with reduced integration and hourglass control) mesh element

with a global seed size of 5mm. The global seed size was determined based on the benchmarked studies and was uniform throughout the model.

The initial geometric imperfection originating from out of straightness of the shape was applied in the FE model by updating the FE model geometry based on the relevant eigenvalue buckling modes. This was done by first performing an eigenvalue buckling analysis on the FE model for 50 eigenmodes. Then, each eigenmode was evaluated for both web and flange buckling. Usually, the first eigenmode exhibited both web and flange buckling and was used to simulate the initial local imperfections of the cross-section. Fig. 4 shows the first eigenvalue buckling mode for the stub column FE model.

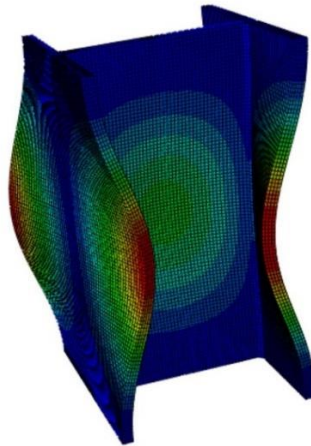


Figure 4: First eigenmode in one of the FE models in 3D

The residual stresses for the FE model were obtained using the following residual stress models from the experimental studies used to benchmark the experimental test: Ban et al. (2013) for 140 ksi (960 MPa) specimens, Cao et al. (2020) for 120 ksi (800 MPa) specimens and Sun et al. (2019) for 100 ksi (690 MPa) specimens. The residual stresses obtained from the models were applied to the cross-section of the FE model using the distribution shown in Table 2. This table shows the equations and the distribution of residual stresses in the developed FE model. Fig. 5 shows the loading setup using the displacement method at the constraint point in one of the FE models.

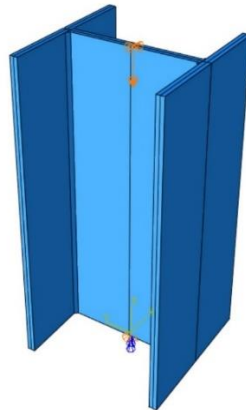


Figure 5: Axial load setup using the displacement method

Table 2: Residual stresses in the FE model

Residual Stress Model	Equations (Units in MPa)	Distribution
Ban et al. (2013)	$\sigma_{frc} = 100 - 930 \left( \frac{1}{\frac{B}{t_f}} \right) - 2205 \left( \frac{1}{t_f} \right)$ $(-960 \leq \sigma_{frc} \leq -96)$ $\sigma_{wrc} = 20 - 2200 \left( \frac{1}{\frac{h_o}{t_w}} \right) - 660 \left( \frac{1}{t_w} \right)$ $(-960 \leq \sigma_{wrc} \leq -96)$ $\sigma_{frt} = \sigma_{wrt} = 460 \text{ MPa}; \sigma_{frte} = 288 \text{ MPa}$	
Cao et al. (2020)	$\frac{B}{t_f} > 6$ $\sigma_{fc} = -670 + 33 \left( \frac{B}{t_f} \right) - 0.5 \left( \frac{B}{t_f} \right)^2$ $(-800 \leq \sigma_{fc} \leq -80)$ $\sigma_{wc} = -550 + 45 \left( \frac{h_o}{t_w} \right) - 1.36 \left( \frac{h_o}{t_w} \right)^2$ $(-800 \leq \sigma_{fc} \leq -80)$ $\sigma_{ft} = \sigma_{wt} = 380 \text{ MPa}$ $\sigma_{fte} = 135 \text{ MPa}$	
Sun et al. (2019)	$f_{ft} = 0.8F_y$ $f_{fc} = 0.8F_y$ $a = 0.225B$ $b = 0.15B$ $c = 0.075h_o$ $d = 0.225h_o$	

### 3. Validation of FE model

The experimental results of Shi et al. (2015) for the 140 ksi stub column, Cao et al. (2020) for the 120 ksi stub column, and Sun et al. (2019) for the 100 ksi stub column were used to validate the FE model. The local buckling load, which is the load that triggers the local buckling failure in columns, can be obtained by two methods from the experiment:

1. Top-of-the-knee method (Hu et al., 1946)
2. Maximum mid-surface strain method (Tillman and Williams, 1989)

The local buckling load according to the top-of-the-knee method is the load corresponding to the top of the knee of the curve of axial load against lateral deflection of the column as shown in Fig.7. If the lateral deflection cannot be measured, any other quantity that increases in substantially the same manner as that of lateral deformation is plotted against load to get the local buckling strength of the column. One such quantity can be differential strain along the axial direction which is consistent with the lateral deformation of the column. In this context, the axial deformation is taken to obtain the local buckling load as shown in Fig. 10. The local buckling load according to the maximum mid-surface strain method is the load corresponding to the maximum mid-surface strain value obtained by the curve of axial load against the mid-surface (center of the column) lateral strain of either the web or the flanges of the column. The maximum mid-surface strain method is most inconsistent as it always assumes that the local buckling takes place at the center of the column which is not really the case in most of the columns. In this paper, the top-of-the-knee method was used to determine the local buckling load of the FE model.

The curves of axial load and lateral displacement and the curves of axial load and engineering strain in the lateral direction of the wide flange specimen were plotted at the mid-height of the specimens and were compared with that of the experimental studies. The obtained curves closely matched the experimental results with less than 10 percent deviation. Fig. 6 displays the comparison of the variation of axial load with strain for the I1 FE model in the flange and the web. Fig. 7 displays the comparison of the variation of axial load with lateral displacement for the I1 FE model in the flange and the web. Fig. 8 displays the comparison of the variation of axial load with strain for the I2 FE model in the flange and the web. Fig. 9 displays the comparison of the variation of axial load with lateral displacement for the I2 FE model in the flange and the web. The obtained curves closely matched the experimental results with less than 10 percent deviation.

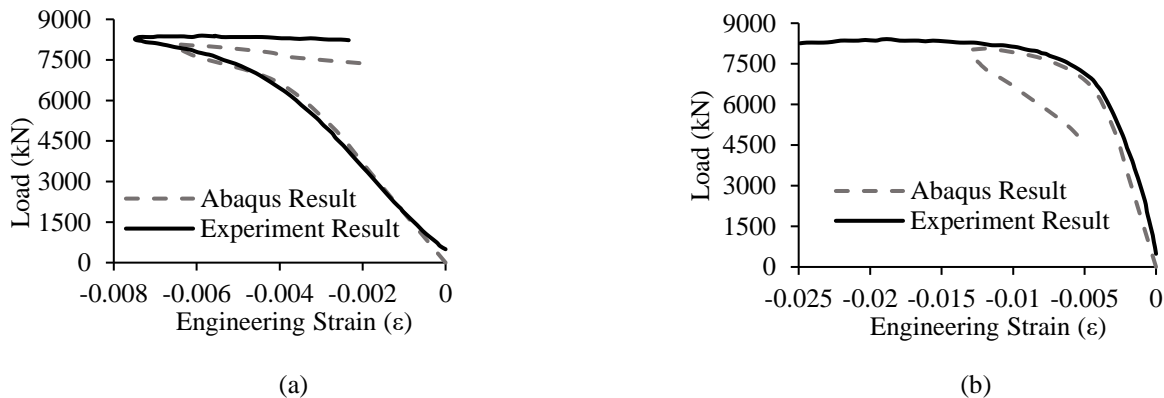
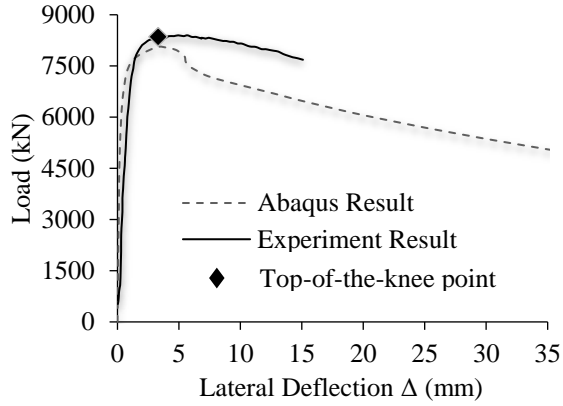
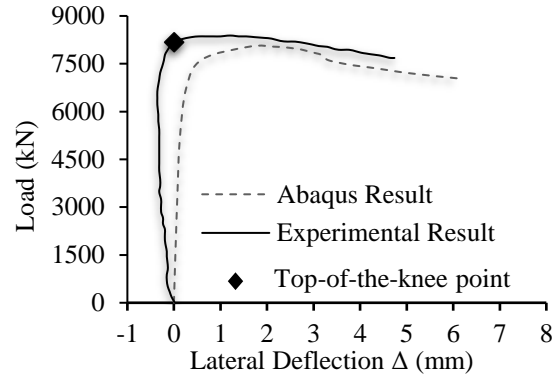


Figure 6: Axial Load vs. Strain in the lateral direction for: (a) flange and (b) web for I1 specimen (1kN = 0.2248 kips)

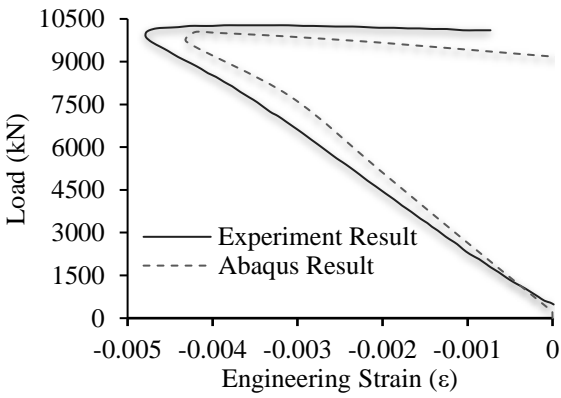


(a)

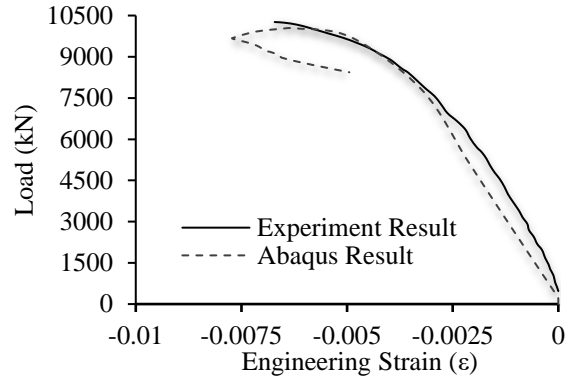


(b)

Figure 7: Axial load vs. lateral deflection for: (a) flange and (b) web for I1 specimen (1kN = 0.2248 kips)

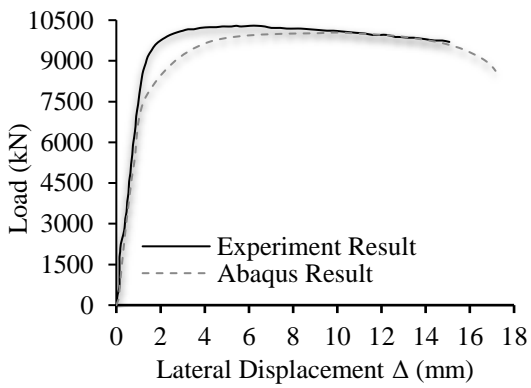


(a)

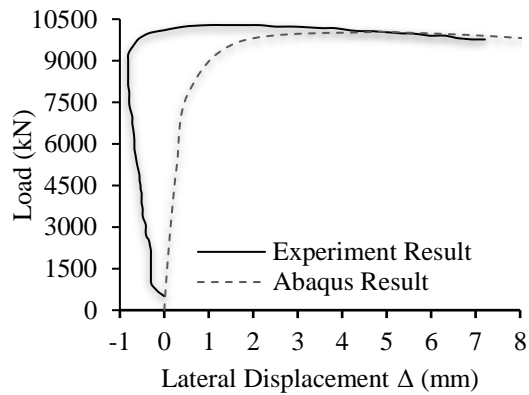


(b)

Figure 8: Axial load vs. strain in the lateral direction for: (a) flange and (b) web for I2 specimen



(a)



(b)

Figure 9: Axial load vs. lateral deflection for: (a) flange and (b) web for I2 specimen

Fig. 10 displays the comparison of the variation of axial load with axial deformation for the I3 and I4 FE models respectively. Table 3 gives a detailed comparison of experimental ultimate load ( $P_{u\text{exp}}$ ) and experimental local buckling load ( $P_{L\text{exp}}$ ) which simulated ultimate load ( $P_{u\text{FE}}$ ) and simulated local buckling load ( $P_{L\text{FE}}$ ) from the FE model. Among the four tests, the mean value of  $P_{u\text{exp}}/P_{u\text{FE}}$  was found to be 1.02 with a standard deviation of 6.46%, and the mean value of  $P_{L\text{exp}}/P_{L\text{FE}}$  was found to be 1.02 with a standard deviation of 6.83%. This shows that the FE model can adequately predict the ultimate load and local buckling load of HS3 stub columns.

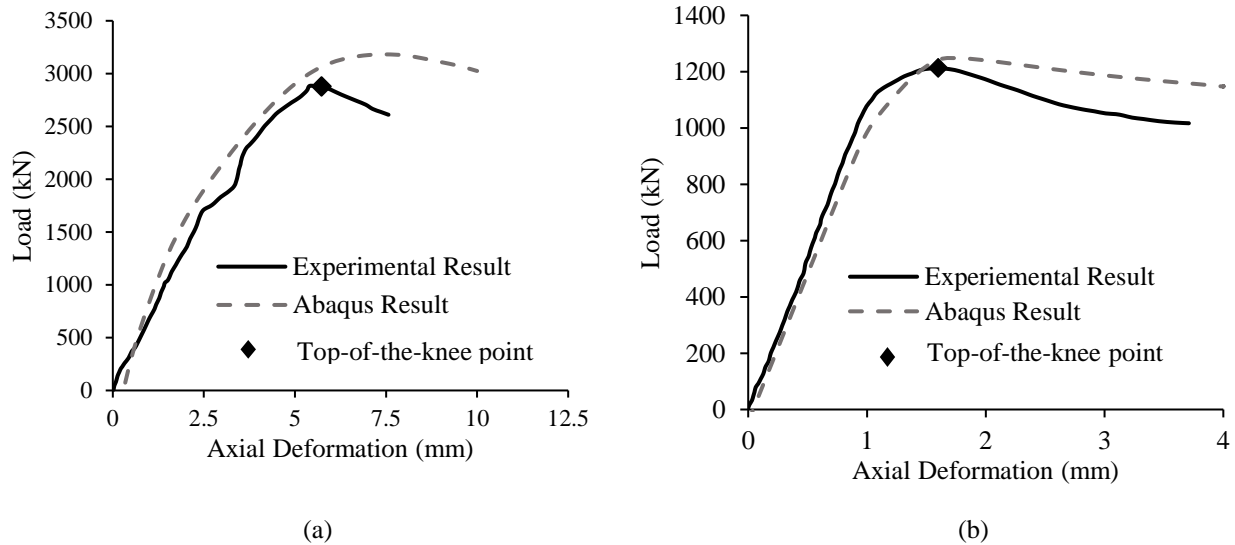


Figure 10: Axial load vs. axial deformation for: (a) I3 - (120ksi) and (b) I4 - (100ksi) specimens

Table 3: Ultimate load and local buckling load comparison

Specimen ID	$F_y$ (ksi)	$P_{u\text{exp}}$ (kN)	$P_{u\text{FE}}$ (kN)	$P_{u\text{FE}}/P_{u\text{exp}}$	$P_{L\text{exp}}$ (kN)	$P_{L\text{FE}}$ (kN)	$P_{L\text{FE}}/P_{L\text{exp}}$
I1	140 (960 MPa)	8389.40	8043.57	0.96	8389.40	8043.57	0.96
I2	140 (960 MPa)	10291.7	10062.5	0.98	10291.7	10034.7	0.98
I3	120 (800 MPa)	2884.00	3182.12	1.10	2850.00	3151.51	1.11
I4	100 (690 MPa)	1214.10	1247.30	1.03	1183.68	1242.70	1.05
Mean				1.02			1.02
COV				6.35%			6.68%

1 kN = 0.2248 kip

#### 4. Parametric study

A parametric study was carried out for three different wide flange built-up sections of grade 100ksi (690 MPa) and 140ksi (960 MPa) across four different kinds of section cross-sections for each column. Table 4 shows the dimensions and other parameters that were varied to determine the ultimate load capacity of each stub column using three initial column sizes: I150×150×5, I320×320×14, and I400×250×7.25. An I150×150×5 column had a width (B) of 150mm (5.9 in.), depth (H) of 150mm (5.9 in.), thickness of both the web and the flange of 5mm (0.197 in.), and an

effective length of 450mm (17.72 in.). These columns closely represent the dimensions of hot-rolled shapes of W6×20, W12×96, and W16×67 sections. It should be noted that column I150×150×5 and its types are atypical given the shallow depth of the column, but they were considered to evaluate the effect of web slenderness on the ultimate load capacity of the column. For each of these columns, the thickness of the flange ( $t_f$ ) and the thickness of the web ( $t_w$ ) were varied while keeping the width and the depth of the original column size the same. Each of the different permutations of column cross-sections was evaluated using 100 ksi and 140 ksi steel material. From these various permutations, a total of twenty-four simulations were performed to study these parameters.

Table 4: Parameters for the ultimate load capacity of the column

Column size (mm x mm x mm)	$F_y$ (ksi)	$t_f$ (in)	$t_w$ (in)
I-150×150×5	100 (690 MPa)	0.276	0.276
I-320×320×14	140 (960 MPa)	0.394	0.394
I-400×250×7.25		0.669	0.551
		0.787	0.669

1 inch = 25.4 mm

The length ( $L$ ) of each column specimen was fixed as per the SSRC (2010) stub column equation, where  $L$  is in inches.

$$L = \min. ((2H + 10), (3H)) \quad (1)$$

Flange slenderness ( $\lambda_f$ ) is the ratio of section width ( $B$ ) to the flange thickness ( $t_f$ ) and web slenderness ( $\lambda_w$ ) is the ratio of section depth ( $h_o$ ) to the web thickness ( $t_w$ ). The combined parameters of flange and web slenderness control the section slenderness of the column. The thickness of each section was varied (keeping the width and depth of the section constant). The limiting width-to-thickness ratios ( $\lambda_r$ ) from AISC 360 (2016) were used to classify each element as slender or non-slender. The I150×150×5 column had slender flanges and a slender web, with both  $\lambda_f$  and  $\lambda_w$  values less than their corresponding  $\lambda_r$  values. The slenderness ratios,  $\lambda_f$  and  $\lambda_w$  were varied to create slender - non-slender, non-slender - slender, and non-slender - non-slender sections with regards to the slenderness of the flange and the slenderness of the web.

Almost all the specimens analyzed using ABAQUS failed by the local buckling mode. The specimen which had non-slender elements of flanges and web failed by flexural buckling mode. The applicability of local buckling equations and flexural buckling equations from AISC 360 (2016) to calculate the nominal compressive strength of the column ( $P_n$ ) were evaluated. The local buckling equations for columns were given by Section E7 of the *Specification* for sections with slender elements and the flexural buckling equations were given by Section E3 of the *Specification*. The nominal compressive strength ( $P_n$ ) for the slender elements is the lowest value based on the critical stress ( $F_{cr}$ ) as determined by the limit states of flexural buckling, torsional buckling, and flexural torsional buckling in interaction with the local buckling. Equation E7-1 gives the expression for  $P_n$  as shown below.

$$P_n = F_{cr} A_e \quad (2)$$

where  $A_e$  is the summation of effective areas of the cross-section obtained by the reduced effective width  $b_e$  and reduced effective depth  $d_e$ , as given by equations E7-2 and E7-3 in the specification.

The results of the twenty-four FE analyses are summarized in the following figures. The load ratio of the ultimate load ( $P_u$ ) obtained by FE analysis and the nominal compressive strength ( $P_n$ ) determined from AISC 360 (2016) were plotted against the interactive slenderness of the column. The interactive slenderness is being defined as  $— (\lambda_f/\lambda_{rf})(\lambda_w/\lambda_{rw})$ , which is calculated as the flange slenderness relative to its limiting ratio multiplied by the web slenderness relative to its limiting ratio. Because both web and flange slenderness varied in this parametric, simply comparing the web slenderness or the flange slenderness did not produce meaningful relationships. The interactive slenderness considers the combined effect of web and flange slenderness on the column behavior. This relationship between load ratio and interactive slenderness is shown in Fig. 11. The load ratio ( $P_u/P_n$ ) was greater than 1.0 for more than 95% of specimens tested, which demonstrated that the nominal strength predicted by AISC 360 (2016) for HS3 stub columns was conservative for both 100 ksi and 140 ksi specimens. The 140 ksi specimens were more conservative than the 100 ksi specimens. There was not much difference in the load ratio ( $P_u/P_n$ ) with low interactive slenderness ( $\leq 2.0$ ). There was a slight increase in load ratio with increase in interactive slenderness greater than 2.0. This suggested that the local buckling equations were slightly more conservative at larger slenderness limits.

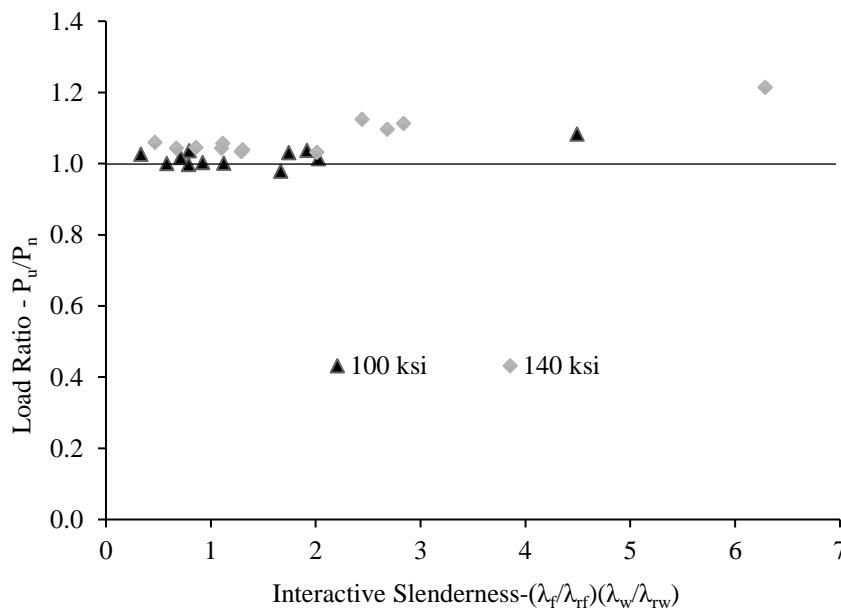


Figure 11: Comparison of load ratio - $P_u/P_n$  and interactive slenderness -  $(\lambda_f/\lambda_{rf})(\lambda_w/\lambda_{rw})$

A plot of load ratio ( $P_u/P_y$ ) against the interactive slenderness of the column is shown in Fig.12 for 100 ksi and 140 ksi specimens.  $P_y$  is the yield load of the specimen obtained from yield stress multiplied by gross cross-sectional area,  $A_g$ . From the graphs in Fig.12, as the interactive slenderness increases, the load ratio ( $P_u/P_y$ ) of the column decreases. This means that as the section slenderness of the column increases, the ultimate load capacity of the column decreased. The

relationship is approximately linear. The load ratio ( $P_u / P_y$ ) is also less than 1.0 for nearly all specimens. This shows that yielding across the entire cross-section has not occurred. This is to be expected in local buckling cases.

Table 5 gives a detailed comparison of simulated ultimate load ( $P_u$ ) and local buckling load ( $P_L$ ) with AISC nominal compressive strength ( $P_n$ ) from the FE model for 100 ksi stub columns. The specimen ID indicates the depth, flange thickness ( $t_f$ ), and web thickness ( $t_w$ ) of the column; for instance, I-150×7×7 represents the original I-150 column from Table 4, with modifications to the flange and web thickness. Similarly, I-320×x×x and I-400×x×x represent the I-320 and I-400 columns, respectively, from Table 5 with modifications to flange and web thickness. The element thicknesses corresponding to each column cross-section are given in Table 5. Among the twelve tests, the mean value of  $P_u / P_n$  was found to be 1.02 with a standard deviation of 2.7%, and the mean value of  $P_L / P_n$  was found to be 1.02 with a standard deviation of 2.6%. The local buckling load and the ultimate load were different for thicker cross-sections and there is a need to study them. The local buckling load was equal to the ultimate load in more than 90% of the cases and was less than the ultimate load, but within 2% for the remaining cases. This meant that the local buckling load ( $P_L$ ) can be used to calculate the strength of the column in all cases. A failure model or a damage data applied to the FE model would give a better picture on the understanding of the relationship between the two quantities.

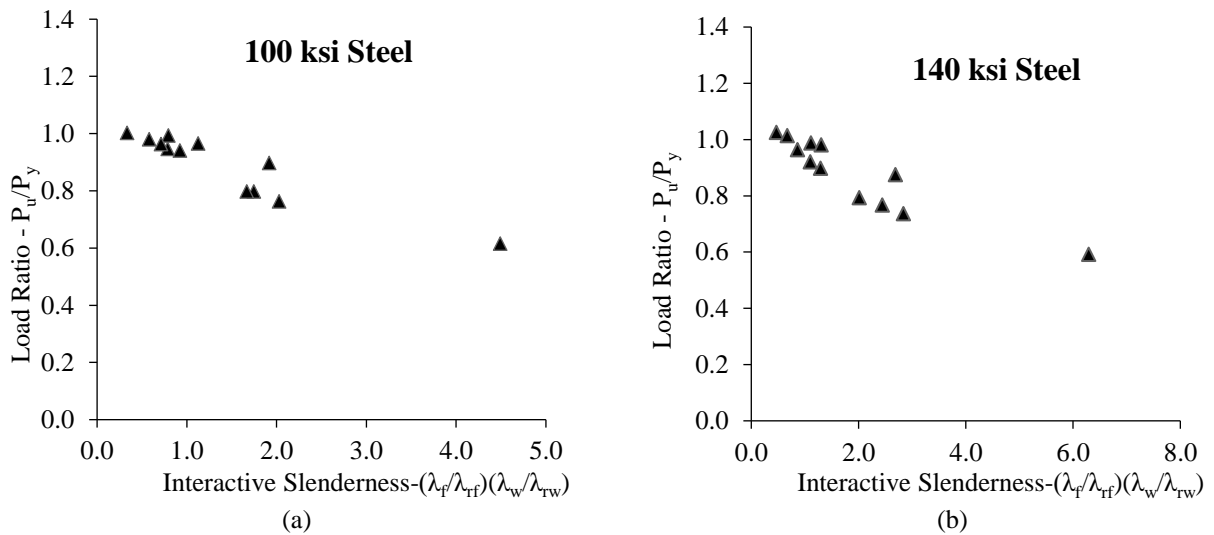


Figure 12: Comparison of load ratio and interactive slenderness for: (a) 100 ksi and (b) 140 ksi columns

Table 6 gives a detailed comparison of simulated ultimate load ( $P_u$ ) and local buckling load ( $P_L$ ) with AISC nominal compressive strength ( $P_n$ ) from the FE model for 140 ksi stub columns. Among the twelve tests, the mean value of  $P_u / P_n$  was found to be 1.08 with a standard deviation of 5.4%, and the mean value of  $P_L / P_n$  was found to be 1.07 with a standard deviation of 4.98%. This means that the design method in the AISC *Specification* can be used in the design of wide flange built-up section columns of grade 100 ksi and 140 ksi.

Table 5: Comparison of AISC compressive strength with ultimate load and local buckling load for 100 ksi steel

Specimen ID (mm × mm × mm)	F <sub>y</sub> (ksi)	P <sub>u</sub> (kip)	P <sub>n</sub> (kip)	P <sub>u</sub> / P <sub>n</sub>	P <sub>L</sub> (kip)	P <sub>L</sub> / P <sub>n</sub>
I-150×5×5	100	280.96	272.54	1.03	280.96	1.03
I-150×7×7	100	459.05	460.34	1.00	459.05	1.00
I-150×10×10	100	679.93	662.80	1.03	679.35	1.03
I-150×10×5	100	573.42	553.32	1.04	573.42	1.04
I-320×14×14	100	1912.36	1907.85	1.00	1912.36	1.00
I-320×10×10	100	1121.13	1106.60	1.01	1109.66	1.00
I-320×17×17	100	2400.71	2401.14	1.00	2391.13	1.00
I-320×17×10	100	2065.56	2063.37	1.00	2065.56	1.00
I-400×7.25×7.25	100	617.95	570.71	1.08	613.60	1.07
I-400×7.25×16	100	1219.58	1246.51	0.98	1219.58	0.97
I-400×16×16	100	2084.78	2049.83	1.02	2084.78	1.02
I-400×16×7.25	100	1492.99	1439.88	1.04	1492.99	1.04
Mean				1.02		1.02
COV				2.65%		2.55%

Table 6: Comparison of AISC compressive strength with ultimate load and local buckling load for 140 ksi steel

Specimen ID (mm × mm × mm)	F <sub>y</sub> (ksi)	P <sub>u</sub> (kip)	P <sub>n</sub> (kip)	P <sub>u</sub> / P <sub>n</sub>	P <sub>L</sub> (kip)	P <sub>L</sub> / P <sub>n</sub>
I-150×5×5	140	378.52	336.75	1.12	378.52	1.12
I-150×7×7	140	625.13	599.00	1.04	625.13	1.04
I-150×10×10	140	974.35	919.44	1.06	970.76	1.06
I-150×10×5	140	798.46	755.60	1.06	798.46	1.06
I-320×14×14	140	2557.30	2475.05	1.03	2546.98	1.03
I-320×10×10	140	1516.05	1362.43	1.11	1489.90	1.09
I-320×20×17	140	3879.64	3719.45	1.04	3848.01	1.04
I-320×20×10	140	3335.56	3212.56	1.04	3314.70	1.03
I-400×7.25×7.25	140	832.81	686.11	1.21	818.93	1.19
I-400×7.25×18	140	1832.90	1777.23	1.03	1829.43	1.03
I-400×16×18	140	3076.64	2945.11	1.05	3069.13	1.04
I-400×16×7.25	140	2039.77	1860.05	1.10	2039.77	1.10
Mean				1.08		1.07
COV				5.02%		4.66%

## 5. Conclusion

FE models generated in ABAQUS were validated through comparison with four HS3 stub columns from the experimental studies of Shi et al. (2015), Cao et al. (2020), and Sun et al. (2019). A parametric study was conducted with this FE model, which included twenty-four stub columns to study the effect of section slenderness on the ultimate load capacity of the column. The ultimate

load capacity and local buckling load for the wide flange stub columns of grade 100 ksi and 140 ksi were established. The numerical results obtained were compared with the design method in AISC *Specification* (2016) to obtain the nominal strength of the column and the applicability of the current local buckling design method in AISC *Specification* (2016) was studied.

The following are the conclusions of this research:

- The local buckling failure was very abundant in slender members, and it did not take place at the center of the column for most of the FE models. The first eigenvalue buckling mode dictated the buckling shape of the column which was in turn dependent upon the end conditions, member, and section slenderness of the column. This meant that the limiting slenderness limits ( $\lambda_r$ ) for CMS given in the AISC *Specification* were applicable for the design of HS3 wide flange sections of grades 100 ksi and 140 ksi.
- The ultimate load capacity of the stub columns decreased with an increase in section slenderness for both 100 ksi and 140 ksi HS3 stub columns.
- For 100 ksi HS3 stub columns, the design method in the AISC *Specification* nearly predicted the nominal strength of the column with a standard deviation of 2.7%. For 140 ksi HS3 stub columns, the design method in the AISC *specification* predicted the nominal strength with a standard deviation of 5.4%. This means that the design method in the AISC *Specification* can be used in the design of wide flange built-up section columns of grade 100 ksi and 140 ksi stub columns. Additional studies are needed to ensure the applicability of the *Specification* for a full range of member sizes and steel grades.

## References

- ABAQUS, (2018), Simulia - Dassault Systemes, Boston, Mass
- AISC, (2010). “ANSI/AISC 360-10: Specification for Structural Steel Buildings.” *American Institute of Steel Construction*, Chicago, Ill.
- AISC, (2016). “ANSI/AISC 360-16: Specification for Structural Steel Buildings.” *American Institute of Steel Construction*, Chicago, Ill.
- Akhtar, M.F., Chicchi, R.A. (2021). “Numerical investigation of the flexural buckling of high strength steel wide flange columns.” *Proceedings of the Annual Stability Conference - Structural Stability Research Council*, Louisville, Kentucky, April 13-16, 2021.
- Ban, H., Shi, G. (2018). “A Review of Research on High-Strength Steel Structures.” *Proceedings of the Institution of Civil Engineers: Structures and Buildings*, 171 (8) 625–41. <https://doi.org/10.1680/jstbu.16.00197>.
- Ban, H., Shi, G., Shi, Y., Bradford, M.A. (2013). “Experimental Investigation of the Overall Buckling Behaviour of 960 MPa High Strength Steel Columns.” *Journal of Constructional Steel Research*, 88 256–66. <https://doi.org/10.1016/j.jcsr.2013.05.015>.
- Ban, H., Shi, G., Shi, Y., Wang, Y. (2012). “Overall Buckling Behavior of 460 MPa High Strength Steel Columns: Experimental Investigation and Design Method.” *Journal of Constructional Steel Research*, 74 (July) 140–50. <https://doi.org/10.1016/j.jcsr.2012.02.013>.
- BSI Eurocode. (2007). “EN 1993-1-12: Eurocode3: Design of Steel Structures: Part 1-12: High Strength Steel.”, BSI, London, UK.
- Cao, X., Gu, L., Kong, Z., Zhao, G., Wang, M., Kim, S.E., Jia, D., Ma, C. (2019). “Local Buckling of 800 MPa High Strength Steel Welded T-Section Columns under Axial Compression.” *Engineering Structures*, 194 (September) 196–206. <https://doi.org/10.1016/j.engstruct.2019.05.060>.
- Cao, X., Zhao, G., Kong, Z., Shen, H., Cheng, C., Chen, Z., Kim, S.E. (2020). “Experimental Study on Local Buckling of 800 MPa HSS Welded I-Section Columns under Axial Compression.” *Thin-Walled Structures*, 155 (October). <https://doi.org/10.1016/j.tws.2020.106878>.
- Chinese Steel Code. (2003). English Version, “GB 50017-2003 Code for Design of Steel Structures (English Version)” *GB 50017-2003 - Code of China*.

- Chinese Steel Code. (2017). English Version, “GB 50017-2017 Code for Design of Steel Structures (English Version)” *GB 50017-2017 - Code of China*. <https://www.codeofchina.com/standard/GB50017-2017.html>.
- Hu, P.C., Lundquist, E.E., Batdorf, S.B. (1946). “Effect of Small Deviations from Flatness of Effective Width and Buckling of Plates and Compression”, *National Advisory Committee for Aeronautics*, NACA TN.1124.
- Schafer, B. (2020). “Research Recommendations: Ad Hoc Task Group on High Strength Steel.” *American Institute of Steel Construction*, Chicago, Ill.
- Seif, M, B Schafer. (2014). “Design of Locally Slender Structural Steel Columns.” *Journal of Structural Engineering*, 140 (4) 04013086. [https://doi.org/10.1061/\(asce\)st.1943-541x.0000889](https://doi.org/10.1061/(asce)st.1943-541x.0000889).
- Shi, G., Hu, F., Shi, Y. (2014). “Recent Research Advances of High Strength Steel Structures and Codification of Design Specification in China.” *International Journal of Steel Structures*, 14 (4) 873–87. <https://doi.org/10.1007/s13296-014-1218-7>.
- Shi, G., Lin, C., Wang, Y., Shi, Y., Liu, Z. (2011). “Finite Element Analysis on the Local Buckling Behavior of High Strength Steel Members under Axial Compression.” In *Advanced Materials Research*, 1477 (82) 243–249. <https://doi.org/10.4028/www.scientific.net/AMR.243-249.1477>.
- Shi, G., Xu, K., Ban, H., Lin, C. (2016). “Local Buckling Behavior of Welded Stub Columns with Normal and High Strength Steels.” *Journal of Constructional Steel Research*, 119 (March) 144–53. <https://doi.org/10.1016/j.jcsr.2015.12.020>.
- Shi, G., Zhou, W., Lin, C. (2015). “Experimental Investigation on the Local Buckling Behavior of 960 MPa High Strength Steel Welded Section Stub Column.” *Advances in Structural Engineering*, 18 (3) 423–37. <https://doi.org/10.1260/1369-4332.18.3.423>.
- Su, A., Sun, Y., Liang, Y., Zhao, O. (2021). “Membrane Residual Stresses and Local Buckling of S960 Ultra-High Strength Steel Welded I-Section Stub Columns.” *Thin-Walled Structures*, 161 (April). <https://doi.org/10.1016/j.tws.2021.107497>.
- Sun, Y., Liang, Y., Zhao, O. (2019). “Testing, Numerical Modelling and Design of S690 High Strength Steel Welded I-Section Stub Columns.” *Journal of Constructional Steel Research*, 159 (August) 521–33. <https://doi.org/10.1016/j.jcsr.2019.05.014>.
- SSRC, (2010). “Guide to Stability Design Criteria for Metal Structures.” *John Wiley & Sons, Inc.*, Hoboken, NJ.
- Tillman, S. C., Williams, A.F. (1989). “Buckling under Compression of Simple and Multicell Plate Columns.” *Thin-Walled Structures*, Vol. 8.
- Usami, T., Fukumoto, Y. (1982). “Local and Overall Buckling of Welded Box Columns.” *ASCE J Struct Div*, 108 (ST3) 525–42. <https://doi.org/10.1061/jsdeag.0005901>.
- Usami, T., Fukumoto, Y. (1984). “Welded Box Compression Members.” *Journal of Structural Engineering*, 110 (10) 2457–70. [https://doi.org/10.1061/\(asce\)0733-9445\(1984\)110:10\(2457\)](https://doi.org/10.1061/(asce)0733-9445(1984)110:10(2457)).